

# Usher syndrome IIIA gene clarin-1 is essential for hair cell function and associated neural activation<sup>†</sup>

Ruishuang Geng<sup>1,‡</sup>, Scott F. Geller<sup>3,‡</sup>, Toshinori Hayashi<sup>4</sup>, Catherine A. Ray<sup>4</sup>, Thomas A. Reh<sup>4</sup>, Olivia Bermingham-McDonogh<sup>4</sup>, Sherri M. Jones<sup>5</sup>, Charles G. Wright<sup>6</sup>, Sami Melki<sup>1</sup>, Yoshikazu Imanishi<sup>2</sup>, Krzysztof Palczewski<sup>2</sup>, Kumar N. Alagramam<sup>1,‡\*</sup> and John G. Flannery<sup>3,‡</sup>

<sup>1</sup>Department of Otolaryngology Head & Neck Surgery and <sup>2</sup>Department of Pharmacology, Case Western Reserve University, Cleveland, OH, USA, <sup>3</sup>Helen Wills Neuroscience Institute, University of California, Berkeley, CA 94720-3190, USA, <sup>4</sup>Department of Biological Structure, University of Washington, Seattle, WA 98195, USA, <sup>5</sup>Department of Communication Sciences and Disorders, East Carolina University, Greenville, NC 27858, USA and <sup>6</sup>Department of Otolaryngology Head & Neck Surgery, Southwestern Medical Center, Dallas, TX 75235, USA

Received March 17, 2009; Revised and Accepted April 29, 2009

**Usher syndrome 3A (USH3A) is an autosomal recessive disorder characterized by progressive loss of hearing and vision due to mutation in the clarin-1 (*CLRN1*) gene. Lack of an animal model has hindered our ability to understand the function of *CLRN1* and the pathophysiology associated with USH3A. Here we report for the first time a mouse model for ear disease in USH3A. Detailed evaluation of inner ear phenotype in the *Clrn1* knockout mouse (*Clrn1*<sup>-/-</sup>) coupled with expression pattern of *Clrn1* in the inner ear are presented here. *Clrn1* was expressed as early as embryonic day 16.5 in the auditory and vestibular hair cells and associated ganglionic neurons, with its expression being higher in outer hair cells (OHCs) than inner hair cells. *Clrn1*<sup>-/-</sup> mice showed early onset hearing loss that rapidly progressed to severe levels. Two to three weeks after birth (P14–P21), *Clrn1*<sup>-/-</sup> mice showed elevated auditory-evoked brainstem response (ABR) thresholds and prolonged peak and interpeak latencies. By P21, ~70% of *Clrn1*<sup>-/-</sup> mice had no detectable ABR and by P30 these mice were deaf. Distortion product otoacoustic emissions were not recordable from *Clrn1*<sup>-/-</sup> mice. Vestibular function in *Clrn1*<sup>-/-</sup> mice mirrored the cochlear phenotype, although it deteriorated more gradually than cochlear function. Disorganization of OHC stereocilia was seen as early as P2 and by P21 OHC loss was observed. In sum, hair cell dysfunction and prolonged peak latencies in vestibular and cochlear evoked potentials in *Clrn1*<sup>-/-</sup> mice strongly indicate that *Clrn1* is necessary for hair cell function and associated neural activation.**

## INTRODUCTION

Usher syndrome is the most common cause of sensory impairment wherein deafness and blindness occur together. It is clinically subdivided into three types based on the degree of deafness and the presence of vestibular dysfunction (1). USH1 is the most severe form and is characterized by profound congenital hearing loss and vestibular dysfunction combined with pre-pubertal onset of retinitis pigmentosa (RP). In

USH2 hearing loss is milder, the onset of RP is after puberty and vestibular function is unaffected. USH3 patients show progressive hearing loss and variable degrees of vestibular dysfunction.

At least 13 loci have been linked to the three types of Usher syndrome, including one locus linked to USH3 (<http://webh01.ua.ac.be/hhh/>). Genes associated with many of these loci have been identified and they encode proteins that belong to diverse classes of proteins (2,3). *CLRN1*

\*To whom correspondence should be addressed at: 11100 Euclid Ave., CWRU, Cleveland, OH 44106; USA. Tel: +1 2168447261; Fax: +1 2169830284; Email: [kna3@case.edu](mailto:kna3@case.edu)

<sup>†</sup>This work is dedicated to Cindy Elden. We appreciate the vision, inspiration and generosity of the Elden family that made this work possible.

<sup>‡</sup>The authors wish it to be known that, in their opinion, the first two authors should be regarded as joint First Authors and the last two authors should be regarded as joint Senior Authors.

(USH3A), the only member of USH3, codes for a four transmembrane-domain protein (4) belonging to a large family of transmembrane proteins which include both the tetraspanin and the claudin families. Members of this family participate in a variety of functions including regulating cell morphology, motility, invasion, fusion and signaling (5–7). Tetraspanins are known to form homo-multimers leading to the assembly of microdomains that interact and nucleate the congregation of other non-tetraspanin membrane proteins. CLRN1 shares some of the features common to tetraspanin proteins, including the predicted four transmembrane domain topology, and very short intracellular loops. This protein may play a vital role in creating and assembling membrane microdomains involved in adhesion strengthening and signaling (7). However, the precise function of CLRN1 in the inner ear is not known.

Several different mutations of human *CLRN1* have been found that cause progressive hearing loss with variable penetrance linked to the N48K mutation, or profound hearing impairment linked to the Y176 stop mutation (4). Similarities between CLRN1 and the calcium channel gamma subunit protein 2 (CACNG2, stargazin) have been proposed (4). Stargazin has been shown to play a key role in the shaping and maintenance of cerebellar synapses (8). However, *in vivo* studies are needed to reveal the molecular mechanism that underlies CLRN1 function. USH3 is inherited in a recessive pattern, suggesting that the loss of function is the cause of the disease. Therefore, studies of the *Clrn1*-null mouse should provide insights into the involved pathogenic mechanisms. Here we report a detailed analysis of the *Clrn1*<sup>-/-</sup> mouse inner ear phenotype and describe the expression pattern of *Clrn1* in the vestibular and cochlear neuroepithelia. Our results suggest that *Clrn1* plays a novel role in hair cell development and function.

## RESULTS

### Clarín-1 is expressed in hair cells and ganglion cells of the inner ear

To determine the expression pattern of *Clrn1* in the cochlear and vestibular hair cells, we carried out mRNA *in situ* hybridization at embryonic (E) stages 16.5, 18.5 and postnatal (P) day 0, 3 and 5. *Clrn1* was found to be expressed as early as E16.5 in the inner ear, in hair cells of the auditory and vestibular sensory epithelia and in the spiral ganglion neurons. Expression was most apparent in the spiral ganglion cells (SGCs) and in the hair cells of the basal turn of the cochlea compared with apical turns at early stages, suggesting the time and location of the onset of *Clrn1* expression (Fig. 1). Hair cell-specific genes typically are initially expressed in the more mature hair cells in the basal cochlea and spread to the apical hair cells with continued development, paralleling the gradient in hair cell maturation. By E18.5, all cochlear hair cells expressed *Clrn1*, with a higher level of expression in the outer hair cells (OHCs) as compared to inner hair cells (IHCs) (Fig. 1). Expression of *Clrn1* was detected by *in situ* hybridization in the inner ear of all stages analyzed, i.e. from both E16.5 to P5, confirming previously reported *in situ* data (4), and from P30 and P60 by RT-PCR (Fig. 3D).

*Clrn1* was also expressed in the vestibular hair cells and Scarpa's ganglion cells. Closer examination of the *Clrn1* labeling in the embryonic saccule revealed strong expression in the hair cells and a much weaker expression in Scarpa's ganglion cells (Fig. 2).

### Generation of *Clrn1*<sup>-/-</sup> mice

To study the function of *Clrn1*, a transgenic mouse lacking the first coding exon (exon 1) of this gene was produced by homologous recombination (Fig. 3A and B). Normal Mendelian segregation of the *Clrn1* exon 1 deleted allele (wild-type *Clrn1*<sup>+/+</sup>, heterozygous *Clrn1*<sup>+/-</sup> and homozygous *Clrn1*<sup>-/-</sup>) was observed. Lack of *Clrn1* expression in the inner ears of *Clrn1*<sup>-/-</sup> mice was confirmed by RT-PCR at various time points from birth well into adulthood (P0–P60) (data from time points P30 and P60 are shown in Fig. 3C and D). *In situ* hybridization of cochlear duct sections from *Clrn1*<sup>-/-</sup> mice confirmed absence of *Clrn1* expression in hair cells and SGCs (Fig. 3E). These results demonstrate that *Clrn1* mRNA is not expressed in the inner ear of the *Clrn1*<sup>-/-</sup> mouse.

We also confirmed the lack of full-length *Clrn1* expression in the retina of the *Clrn1*<sup>-/-</sup> mouse (data not shown). In *Clrn1*<sup>-/-</sup> mice, though, we failed to discover the deficiencies in structural abnormality of photoreceptors and other neurons at the age of 4 months (data not shown). Furthermore, electroretinograms (ERG) analyses did not reveal the sign of photoreceptor degeneration up to the age of 16 months, as exemplified by the lack of significant differences in the a-wave amplitudes at various light conditions (Fig. 4).

### *Clrn1*<sup>-/-</sup> mice show progressive hearing loss

To assess hearing function in *Clrn1*<sup>-/-</sup> mice, we performed auditory brainstem response (ABR) tests on mice of different ages starting at P21, the age at which the auditory system in mice becomes fully mature. ABR tests reflect the electrical responses of both the cochlear ganglion neurons and the nuclei of the central auditory pathway to sound stimulation. About ~30% of *Clrn1*<sup>-/-</sup> mice showed elevated ABR thresholds (Fig. 5A), but the majority (~70%) failed to produce detectable ABR responses at P21. As expected, *Clrn1*<sup>+/+</sup> littermates produced characteristic ABR waveforms (peaks 1–4) at thresholds from 25 to 45 dB peSPL (decibel peak equivalent Sound Pressure Level) for pure tones 8–32 kHz (Fig. 5A); *Clrn1*<sup>+/-</sup> mice showed similar results (data not shown). Interestingly, in the recordings from mutant mice, response peak latencies were significantly prolonged compared with controls for all four peaks. For example, at 8 kHz the initial response peak (peak 1) occurred at ~2.0 ms in *Clrn1*<sup>+/+</sup> mice, but it was close to 3 ms in the *Clrn1*<sup>-/-</sup> mice (Fig. 5B). The interpeak latencies P1–P2 and P1–P3 were also prolonged in the mutants compared with control siblings (Table 1). By P30, hearing function was not detectable in any *Clrn1*<sup>-/-</sup> mice tested (data not shown). These results suggest that *Clrn1*<sup>-/-</sup> mice have some auditory function at young ages but lose it rapidly after P21. This prompted us to test mutants at time points earlier than P21. All of six *Clrn1*<sup>-/-</sup> mice tested at P14 and P20 showed

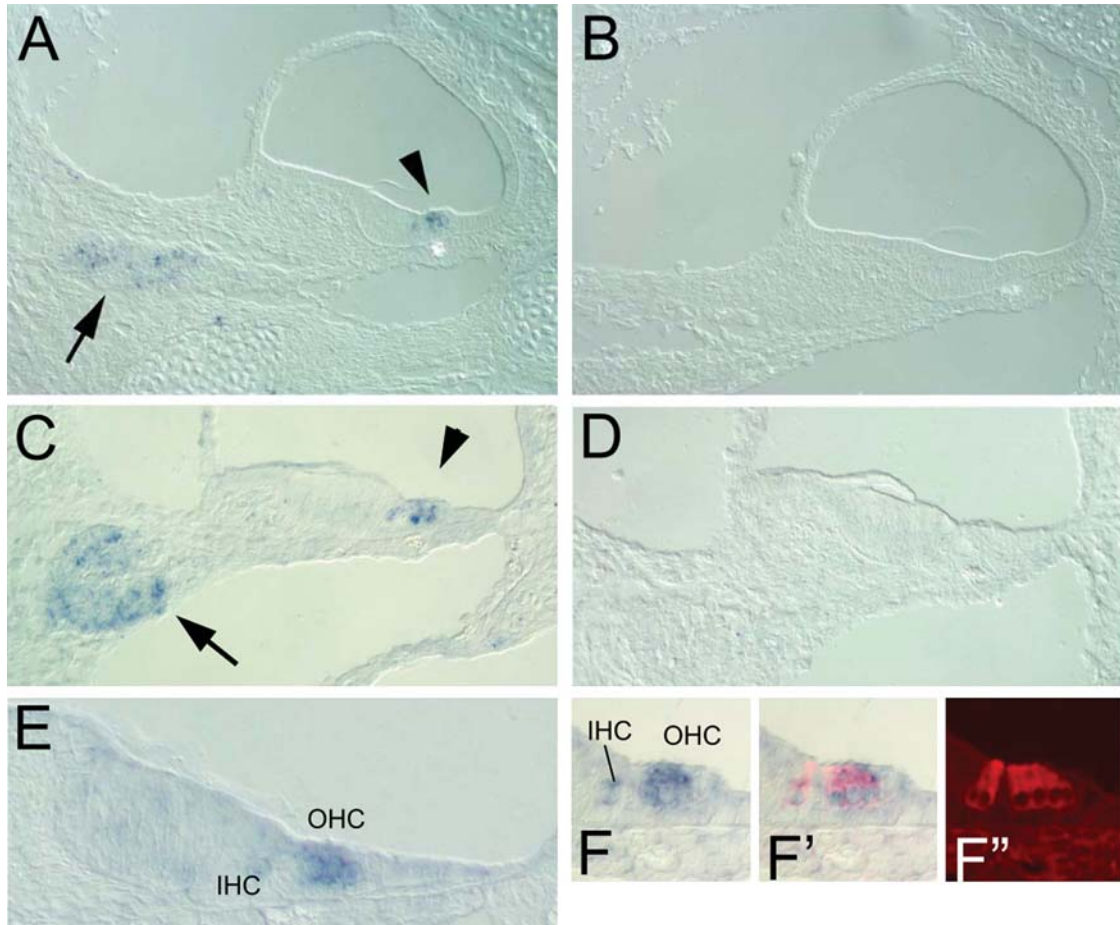


**Figure 1.** Expression of *Clrn1* in the mouse cochlea detected using *in situ* hybridization. (A and B) Antisense (A) and sense (B) probes used to localize *Clrn1* at E18 in the middle turn. (C and D) Antisense (C) and sense (D) probes used to localize *Clrn1* at P3 in the middle turn. Arrows point to the expression in the spiral ganglion, while arrowheads point to expression in the hair cells. (E and F–F'') Expression of *Clrn1* in hair cells was confirmed at E18 by post-*in situ* antibody labeling with anti-myosin VI. (F, F'') *Clrn1* is expressed more highly in the outer hair cells (OHC) than in the inner hair cells (IHC).

some hearing function; however, thresholds were significantly elevated and peak latencies prolonged (Table 2). The increased intensity of sound needed to elicit a response from mutant ears at P14–21 suggests diminished hair cell function early in the life of *Clrn1*<sup>-/-</sup> mice and the prolonged P1 latency implies a delay in neural activation.

#### Loss of OHC function in *Clrn1*<sup>-/-</sup> mice

To determine whether the hearing impairment in *Clrn1*<sup>-/-</sup> mice specifically involved an OHC defect, we recorded distortion product otoacoustic emissions (DPOAEs) which are indicative of OHC amplification activity. At P21, *Clrn1*<sup>-/-</sup> mice produced no detectable DPOAEs above the noise floor (NF) (Fig. 5C and D). Although, more than 10 *Clrn1*<sup>-/-</sup> mice with high threshold ABR, similar to those tested in Figure 5A and B, were tested at P21, we were unable to record any DPOAEs from these mutants. In contrast, wild-type controls showed normal DPOAE responses (Fig. 5C and D). Absence of DPOAEs at a very young age clearly indicates lack of OHC function in *Clrn1*<sup>-/-</sup> mice.

In summary, our hearing assessments are consistent with a cochlear lesion site and a sensorineural hearing loss. Further, auditory results show that *Clrn1*<sup>-/-</sup> mutation affects hair cell function, and either hair cell to afferent nerve communication or primary afferent neural activation.

#### *Clrn1*<sup>-/-</sup> mice show progressive loss of balance function

In *Clrn1*<sup>-/-</sup> mice, balance function was not overtly/severely affected by P30. In contrast, circling and head bobbing activity in the Usher 1F model is evident as early as P12 and becomes more obvious with age (9,10). The head bobbing phenotype in *Clrn1*<sup>-/-</sup> mice is mild and variable at young ages (P21–40) with some mutants indistinguishable from their wild-type siblings. However, vestibular dysfunction became more apparent with age such that some *Clrn1*<sup>-/-</sup> mice evidenced clearer signs of head bobbing than others by 6 months of age. Young adult (P21–P90) mutants were subjected to swim tests along with controls. Generally, *Clrn1*<sup>-/-</sup> mice appeared less stable in the water compared with controls (*Clrn1*<sup>+/+</sup> or *Clrn1*<sup>+/-</sup>), tending to roll from one side to the other, even though they used their tails effectively to remain prone in

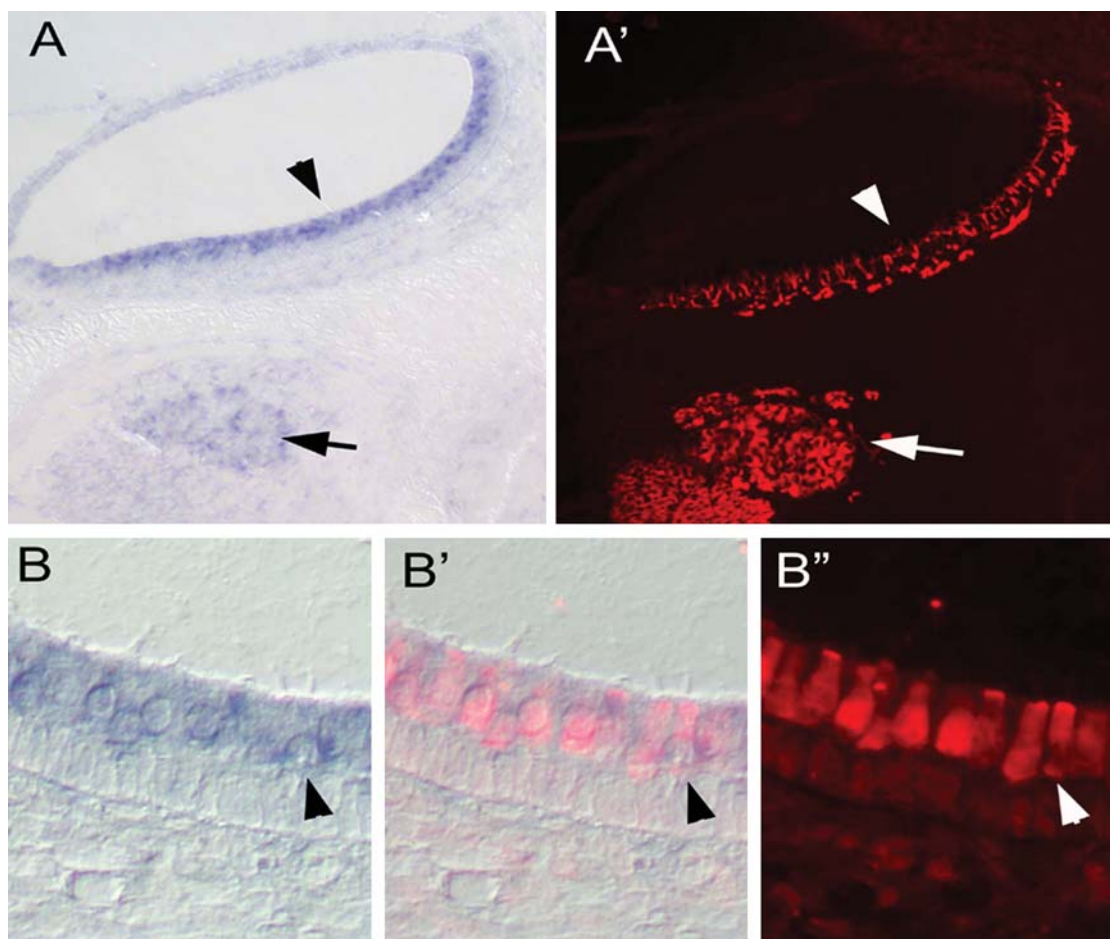


**Figure 2.** Expression of *Clnr1* in the mouse saccule detected using *in situ* hybridization. (A and A') *Clnr1* is expressed in vestibular hair cells (arrowhead) and ganglion neurons, as shown in (A') using post-*in situ* immunolabeling with anti-TuJ1 antibody (arrow). (B and B') Higher magnification view of *Clnr1* expression in vestibular hair cells co-labeled with myosin VI. (B' and B'') Arrowhead points to an example of a double-labeled cell.

the water. But abnormal swimming behavior was not discernable in all tested *Clnr1*<sup>-/-</sup> mice which prompted us to quantify vestibular function in these knockout (KO) animals.

To quantitatively examine vestibular function in *Clnr1*<sup>-/-</sup> mice, we recorded vestibular evoked potentials (VsEP) of *Clnr1*<sup>-/-</sup> and *Clnr1*<sup>+/+</sup> mice at P21–P30. It should be noted that VsEP recordings with linear stimulation specifically assess the otoconial organs (utricle and saccule). On average, VsEP thresholds of *Clnr1*<sup>-/-</sup> mice ( $-5.5 \pm 3.6$  dB re: 1.0 g/ms) were significantly higher than those of *Clnr1*<sup>+/+</sup> controls ( $-11.0 \pm 1.2$  dB re: 1.0 g/ms), although the *Clnr1*<sup>-/-</sup> mice showed greater variability in their response thresholds ( $t = -3.5$ ,  $P = 0.012$ ). Some *Clnr1*<sup>-/-</sup> mice had normal VsEP thresholds, but all evidenced abnormalities in response peak latencies (Fig. 6A). P1 peak latencies were significantly prolonged ( $t = 2.26$ ,  $P = 0.00003$ ) (Fig. 6B and Table 2).

In short, albeit more gradually apparent, the overall characteristics of the vestibular phenotype are similar to those observed in the auditory system of the *Clnr1*<sup>-/-</sup> mice, thus confirming that the organ of Corti and the saccular and utricular sensory receptors of the inner ear are affected. This strengthens our conclusion that disabling mutations in *Clnr1* affect hair cell function and either hair cell to afferent nerve

communication or primary afferent neural activation. However, no significant change in the vestibular hair cell morphology was observed within P21–30 (data not shown). Changes in the vestibular system tend to progress much more slowly than in the cochlea as noted above. Therefore, it will be necessary to examine older (>P30) *Clnr1*<sup>-/-</sup> mice carefully before we come to any conclusion about the effect of *Clnr1* mutation on vestibular hair cells morphology.

#### The stereocilia of OHCs are defective in *Clnr1*<sup>-/-</sup> mice

To better understand the structure–function relationship in *Clnr1*<sup>-/-</sup> mice, we examined organs of Corti from young animals by scanning electron microscopy (SEM). Stereocilia display a 'V' shaped configuration on the OHCs and a crescent shaped configuration on the IHCs in normal mice by P10. There were obvious abnormalities in the arrangement of stereocilia in *Clnr1*<sup>-/-</sup> mice as compared to controls as early as P2 (Fig. 7A and B). Abnormalities similar to those observed at P2 were also noted in OHC stereocilia at P6 (Fig. 7C and D). By P10, the derangement of the stereocilia was more apparent compared with the well organized, mature stereocilia bundles typically observed in the control

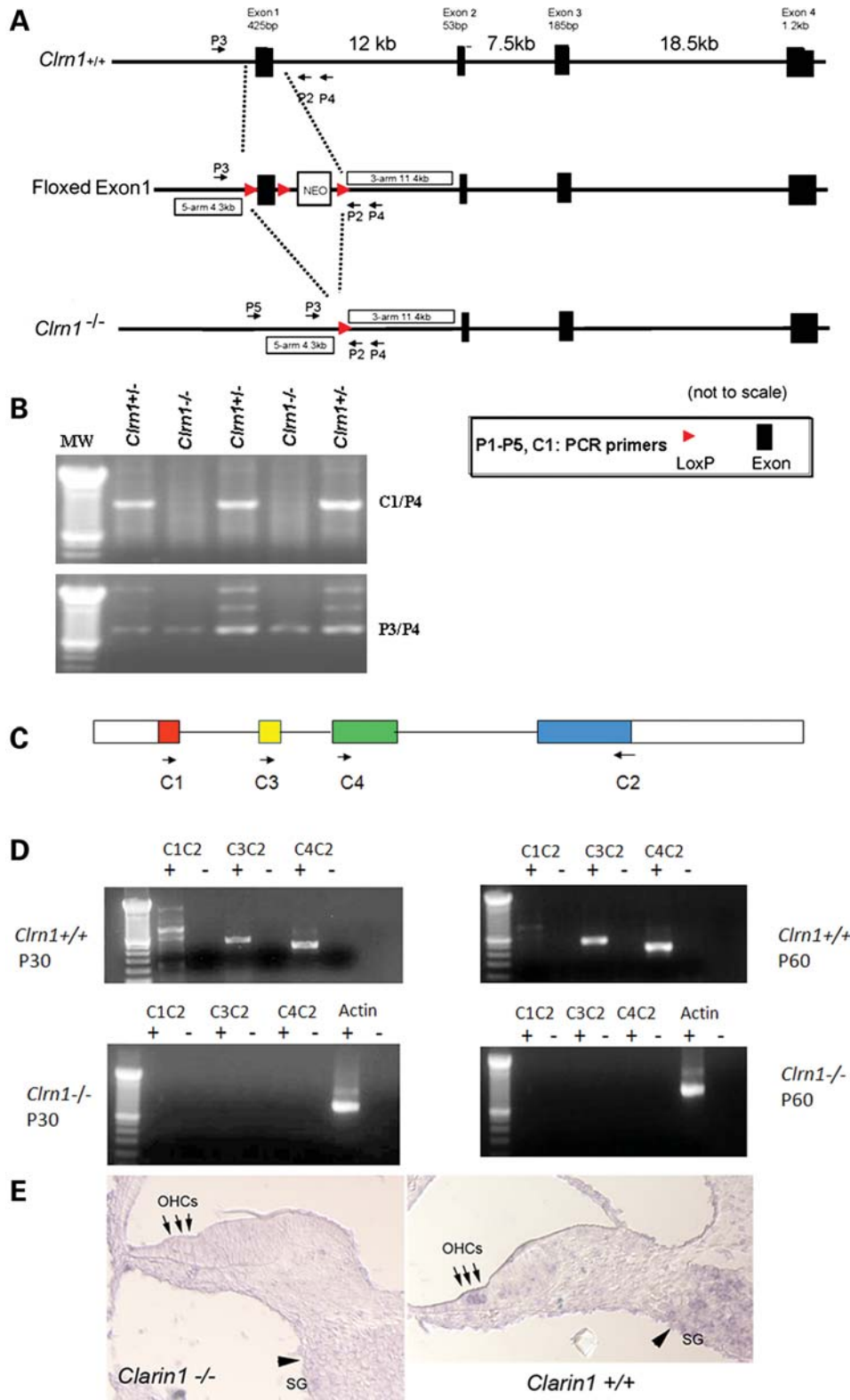


**Figure 3.** Generation *Clrn1* transgenic knockout. (A) Map of the targeted exon, targeting construct and excision of exon 1 after exposure to cre recombinase. (B) PCR-based genotyping to identify mice heterozygous (+/-) or homozygous (-/-) for the KO allele. PCR products amplified using C1/P4 or P3/P4 primers resolved on agarose gel. (C) Exon-intron map of *Clrn1* and location of RT-PCR primers. (D) RT-PCR analysis of *Clrn1* expression in wild-type and KO cochlea at P30 and 60. (E) shows *in situ* hybridization of *Clrn1* mRNA in wild-type or *Clrn1*<sup>-/-</sup> mouse cochlea. Antisense probe used to localize *Clrn1* in the middle turn of the cochlea at P1. Arrows point to the expression in the outer hair cells (OHCs), while arrowheads point to expression in the spiral ganglion (SG) cells. *Clrn1* expression is absent in the KO mouse.

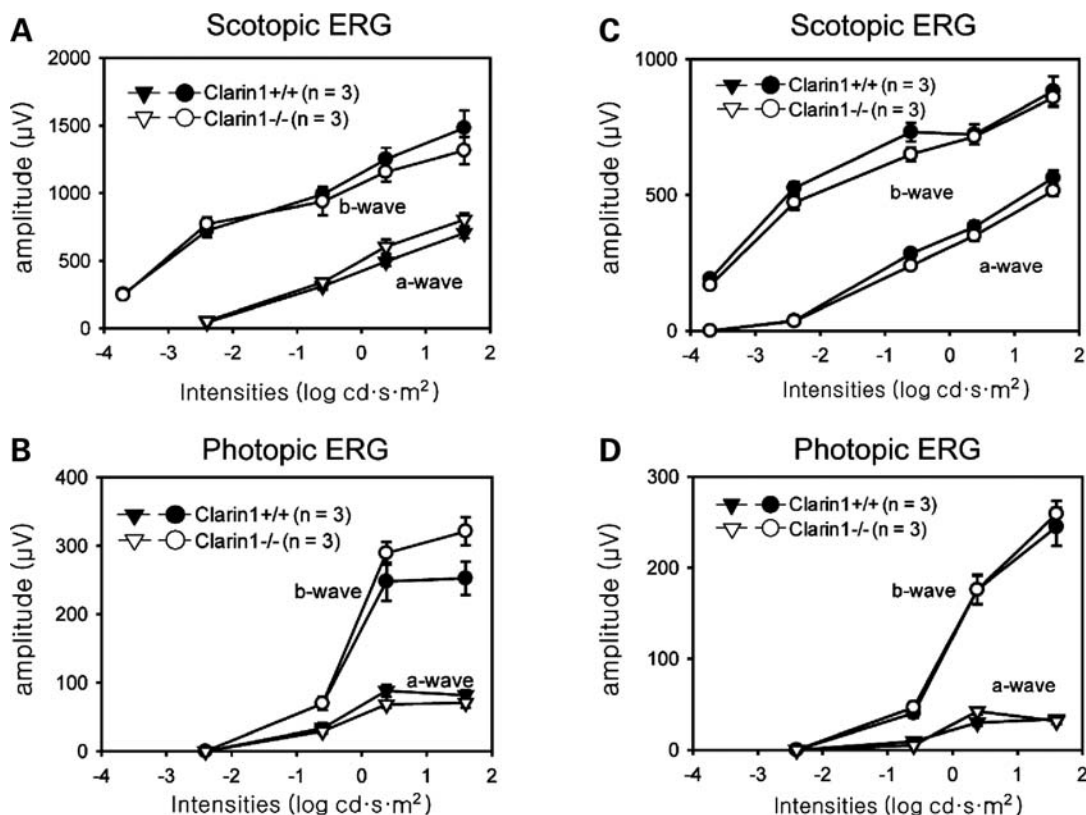


**Figure 4.** ERG responses of *Clrn1*<sup>-/-</sup> mouse. (A and B) ERG responses of 8-month-old mice. (C and D) ERG responses of 16-month-old mice. Under both scotopic and photopic conditions, there were no significant differences in ERG responses between *Clrn1*<sup>-/-</sup> and *Clrn1*<sup>+/+</sup> mice.

specimen at P10 (Fig. 7E and F). In addition to general disorganization of the bundles, circular clusters of abnormal stereocilia were also seen on some OHC (Fig. 7F). Stereocilia defects of the same type and approximate severity also were present at P15 and the basal and upper cochlear turns appeared to be similarly affected (Fig. 7G and H). There was little progression in the severity of stereocilia defects during the period from P2 to P15, suggesting that progression of this pathology is relatively slow during that interval. In all cases, the stereocilia of IHCs appeared normal or only mildly affected. The severity of stereocilia defects in OHCs varied among *Clrn1*<sup>-/-</sup> mice, consistent with the variable severity of hearing loss in different animals.

#### Disabling mutation in *Clrn1* leads to cochlear hair cell death

The rapidly progressive hearing loss observed in *Clrn1*<sup>-/-</sup> mice suggests that degeneration of cochlear hair cells may occur at a relatively early age. Accordingly, the cochleas of *Clrn1*<sup>-/-</sup> and control mice were examined in histological cross sections at P21 and P30. In cochlear cross sections, loss of OHCs was apparent by P21 in *Clrn1*<sup>-/-</sup> mice as compared to wild-type specimens (Fig. 8A and B). By P30, almost all OHCs and IHCs were missing throughout most of the cochlea in *Clrn1*<sup>-/-</sup> mice (Fig. 8C and D), whereas these hair cells were well maintained in wild-type mice. The sup-

porting cells were also degenerated in the basal turn, leading to collapse of the organ of Corti.

#### DISCUSSION

The use of gene knockout technology in the mouse is a powerful approach for study of diseases such as USH3A. One of the most common mutations in USH3A patients is the Y176X mutation in *CLRN1*. The premature stop codon present in Y176X would result in a small truncated protein that is most likely functionally inactive or null. Therefore, we hypothesized that the inner ear phenotype in *Clrn1*-null mouse would be similar to the clinical presentation of patients harboring the Y176X mutation. Our results show that *Clrn1*<sup>-/-</sup> mice display early onset hearing loss that rapidly progresses to a profound loss by ~P30. In contrast, vestibular dysfunction was relatively mild in young animals, progressing slowly (relative to hearing loss) to a severe deficit with age. The overall inner ear phenotype in the *Clrn1*<sup>-/-</sup> mouse is similar to the inner ear dysfunction observed in USH3A patients with a presumptive null mutation in *CLRN1*. As with other Usher mouse models, we failed to detect any obvious retinal dysfunctions in *Clrn1*<sup>-/-</sup> mouse. Therefore, the KO mouse reported here should be a good model for the ear disease occurring in human USH3A patients.

*Clrn1*<sup>-/-</sup> mice showed early onset (P14–21) hearing loss with elevated ABR thresholds of 85–95 dB peSPL. In addition, the absolute latencies of all ABR waves and the

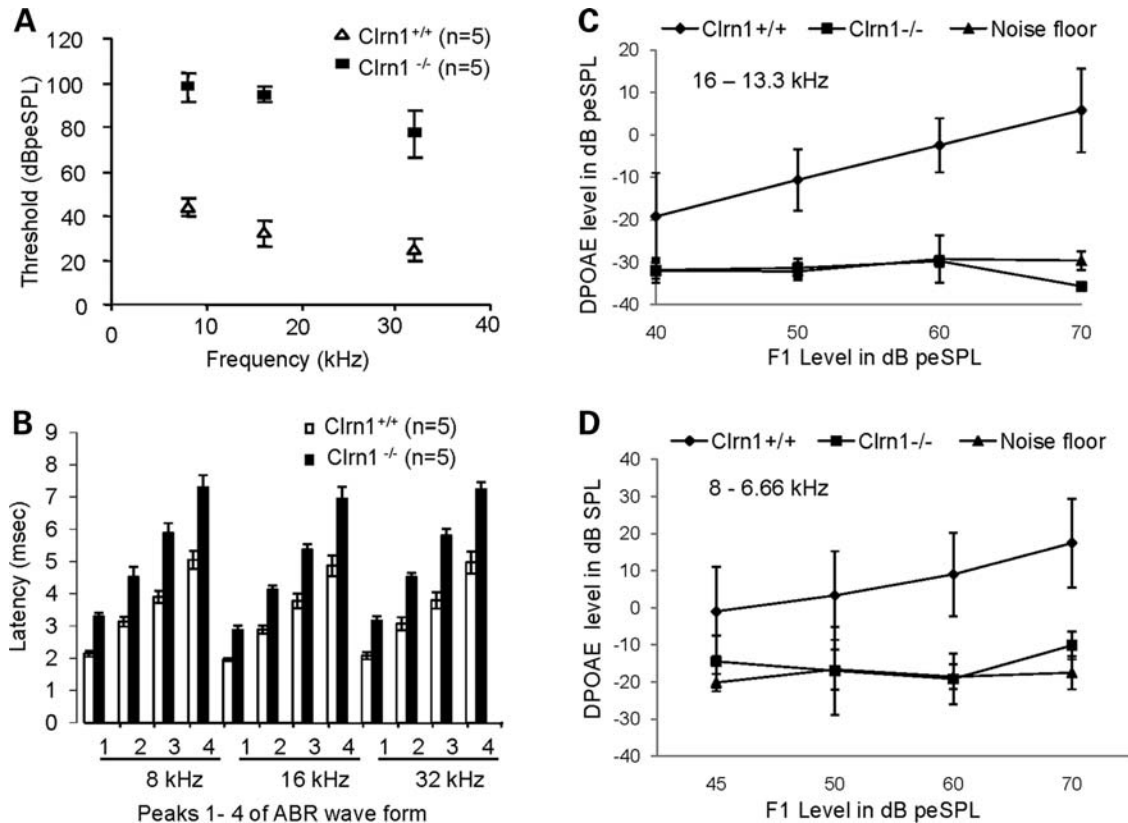


**Figure 5.** Assessment of hearing impairment in *Clnr1*<sup>-/-</sup> mice at P21. ABR: (A) shows that the mean ABR thresholds *Clnr1*<sup>-/-</sup> mice are significantly elevated compared with *Clnr1*<sup>+/+</sup> mice at 8, 16 and 32 kHz. (B) shows significant delay in latency of peaks 1–4 in *Clnr1*<sup>-/-</sup> mice compared with *Clnr1*<sup>+/+</sup> mice at 8, 16 and 32 kHz. DPOAE: Assessment of OHC functions in *Clnr1*<sup>-/-</sup> mice. (C and D) Represent input/output (I/O) function test: the input at F1 (x-axis) plotted against the output, represented as mean (and mean  $\pm$  SD) DPOAE levels (y-axis), at two pairs of frequency: 16–13.3 and 8–6.6 kHz. For I/O test, data were averaged from five *Clnr1*<sup>+/+</sup> and five *Clnr1*<sup>-/-</sup> mice; results were compared with noise floor average from five trials ( $n = 5$ ).

interpeak latencies between the waves were significantly delayed, suggesting a neural deficit in addition to a hair cell function deficiency. In the vestibular apparatus, gravity receptor function declined more gradually, but the overall profile was in agreement with the cochlear phenotype. Similar to the delayed latency in ABR peaks, prolonged VsEP peak latencies were observed in all *Clnr1*<sup>-/-</sup> mice tested, suggesting a defect in gravity receptor hair cell function and associated neural activation. Prolonged peak latencies seen in *Clnr1*<sup>-/-</sup> mice are reminiscent of mutants with demyelinating disorders (11,12). These findings suggest that the auditory and vestibular deficits in *Clnr1*<sup>-/-</sup> mice are caused by peripheral defects that affect sensory transduction, the communication of hair cells with afferent neurons and/or signal propagation along the eighth nerve. It has been predicted that CLRN1 might play a role in ribbon synapses based on sequence similarities between the CLRN1-specific motif and stargazin, a cerebellum synapse protein (4). The expression of *Clnr1* in hair cells and the functional deficits observed in *Clnr1*<sup>-/-</sup> mice support a possible role for CLRN1 in ribbon synapses. The progressive deterioration in cochlear and vestibular function observed in *Clnr1*<sup>-/-</sup> mice is reminiscent of the clinical ear disorder in USH3A (13,14).

*In situ* mRNA hybridization results confirm the specific expression of *Clnr1* in hair cells and ganglion cells of the cochlea and saccule as early as E16.5 and indicate that this

expression continues during the postnatal period. While stereocilia bundle morphogenesis is still underway at E16.5 (15), this timing also coincides with the onset of mechanotransduction in embryonic hair cells of mice (16). In the cochlea, mRNA *in situ* hybridization shows stronger expression of *Clnr1* in OHCs as compared to IHCs, suggesting a more dominant role for clarin-1 in the OHC, consistent with the fact that DPOAEs are absent in hearing *Clnr1*<sup>-/-</sup> mice. SEM studies also provide strong support for early onset OHC defects in *Clnr1*<sup>-/-</sup> mice. Our results indicate that the auditory phenotype is caused at least in part by hair cell defects and that *Clnr1* is required during hair cell development.

Distinct features of the inner ear phenotype in *Clnr1*<sup>-/-</sup> mice as compared to the phenotype reported in Usher type I and II mouse models suggests a novel inner ear function for CLRN1. Mouse mutants harboring presumptive null mutations in Usher type I genes exhibit severe disorganization of stereocilia during the early stages of IHC and OHC development (17–19), and the progression of stereocilia pathology from P0 to P15 is quite rapid, as exemplified in Usher type 1F models (20,21). In contrast, mice carrying a null mutation in *Clnr1* display relatively less severe stereocilia defects on OHCs in all turns of the cochlea at early postnatal stages, but the progression of severity seems slow from P2 to P15; the stereocilia defects in IHCs are barely detectable at these

**Table 1.** Peak latencies and interpeak latencies of ABR response for *Clrn1*<sup>+/+</sup> and *Clrn1*<sup>-/-</sup> shown earlier (Fig. 5A and B). Absolute and interpeak latencies (measured in ms) were calculated for threshold levels (i.e. 0 dB sensation level). *n* = 5 for each genotype. Data in this table were generated in the laboratory of KA at CWRU

ABR latencies at P21						
peaks	8 kHz <i>Clrn1</i> <sup>+/+</sup>	<i>Clrn1</i> <sup>-/-</sup>	16 kHz <i>Clrn1</i> <sup>+/+</sup>	<i>Clrn1</i> <sup>-/-</sup>	32 kHz <i>Clrn1</i> <sup>+/+</sup>	<i>Clrn1</i> <sup>-/-</sup>
1	2.14 ± 0.09	3.3 ± 0.10	1.96 ± 0.05	2.87 ± 0.14	2.08 ± 0.11	3.16 ± 0.15
2	3.13 ± 0.15	4.52 ± 0.31	2.89 ± 0.12	4.13 ± 0.12	3.07 ± 0.20	4.52 ± 0.13
3	3.9 ± 0.19	5.88 ± 0.31	3.78 ± 0.23	5.37 ± 0.16	3.79 ± 0.25	5.8 ± 0.21
4	5.05 ± 0.28	7.3 ± 0.38	4.87 ± 0.32	6.95 ± 0.36	4.97 ± 0.34	7.24 ± 0.22
P1–P2 <sup>a</sup>	0.99	1.22	0.93	1.26	0.99	1.36
P1–P3 <sup>a</sup>	1.77	2.58	1.82	2.50	1.71	2.64

<sup>a</sup>Latencies and interpeak latencies in ms.**Table 2.** ABR and VsEP response parameters for *Clrn1*<sup>+/+</sup> and *Clrn1*<sup>-/-</sup> mice tested at various ages. Thresholds were measured in dB peSPL for ABR and dB re: 1.0 g/ms for VsEP. Latency was measured in ms and amplitude in  $\mu$ V at equal sensation levels (12 dBSL for ABR and 9 dBSL for VsEPs). The number in parentheses indicates the number of animals tested for each measure. Data in this table were generated in the laboratory of SMJ at ECU

Parameter	Age	ABR (8 kHz) <i>Clrn1</i> <sup>+/+</sup>	<i>Clrn1</i> <sup>-/-</sup>	VsEP <i>Clrn1</i> <sup>+/+</sup>	<i>Clrn1</i> <sup>-/-</sup>
Threshold	14 days	42.2 ± 8.4 (4)	76.5 ± 6.1 (6)	<sup>a</sup>	-4.50 (1)
	20 days	41.0 ± 8.5 (2)	77.0 ± 5.0 (6)	-10.50 ± 0.00 (2)	-5.36 ± 4.49 (7)
	25 days	<sup>a</sup>	NA (10) <sup>b</sup>	-10.50 ± 0.00 (3)	-3.50 ± 4.58 (3) <sup>c</sup>
	30 days	33.6 ± 1.2 (4)	NA (10) <sup>b</sup>	-11.50 ± 1.73 (3)	-6.50 ± 1.73 (3) <sup>c</sup>
P1 latency	14 days	2.04 ± 0.08 (4)	3.26 ± 0.11 (6)	<sup>a</sup>	1.73 (1)
	20 days	2.21 ± 0.10 (2)	3.26 ± 0.18 (6)	1.48 ± 0.12 (2)	1.64 ± 0.15 (7)
	25 days	<sup>b</sup>	NR <sup>a</sup>	1.40 ± 0.06 (3)	1.64 ± 0.04 (3) <sup>c</sup>
	30 days		NR	1.36 ± 0.05 (3)	1.63 ± 0.07 (3) <sup>c</sup>
P1-N1	14 days	3.16 ± 1.23 (4)	1.27 ± 0.24 (6)	<sup>a</sup>	0.66 (1)
	20 days	0.96 ± 0.07 (2)	0.70 ± 0.11 (4)	0.76 ± 0.43 (2)	0.54 ± 0.07 (7)
Amplitude	25 days	<sup>a</sup>	NR	0.44 ± 0.14 (3)	0.46 ± 0.12 (3)
	30 days		NR	0.87 ± 0.30 (3)	0.43 ± 0.08 (3) <sup>c</sup>
	IPL P1–P2	20 days	0.96 ± 0.01 (2)	1.07 ± 0.06 (2)	0.74 ± 0.11 (2)
IPL P1–P3	20 days	2.02 ± 0.01 (2)	2.23 ± 0.11 (2)	1.76 ± 0.14 (2)	Insufficient data

IPL, interpeak latencies. <sup>a</sup>not recorded; <sup>b</sup>No ABR at 100 dB peSPL; <sup>c</sup>significantly different (*P* < 0.05).

ages. This is consistent with the hearing loss phenotype of *Clrn1*<sup>-/-</sup> mice: ~30% of these mutants still have detectable hearing (85–90 dB peSPL) at young ages (P14–21), while Usher type 1 mutants display profound hearing loss at birth. In addition, Usher type 1 mutants show early (P10–P15) onset head bobbing and circling behavior, while young (P21–P30) *Clrn1*<sup>-/-</sup> mice exhibit only mild defects, in most cases requiring VsEP recordings to confirm vestibular dysfunction. Mice carrying mutations in the Usher 2a (*usherin*) gene show hearing loss only at high frequencies and slightly elevated DPOAEs at high frequencies. Concomitantly, usherin mutant mice show hair cell loss only in the basal turn of the cochlea (22). In contrast, mice carrying mutations in the Usher 2d (*whirlin*) gene are deaf and the stereocilia are stunted (23). Usher 2C (*Vlgr1*-mutated) mice carrying targeted deletion of *Vlgr1* are deaf by P21 and stereocilia bundles become disorganized soon after birth (24). Evidence from the recent literature suggests that most, if not all, Usher proteins interact with each other at some level to ultimately mediate their effects on function in hair cell and photoreceptor cell development and function (3,17,25). Evidence in the literature also suggests possible linkage between CLRN1 and Myosin VIIa (Usher 1B gene product).

USH3A patients with a single mutant allele of Usher1B exhibits USH1 phenotype (26). Myosin VIIa has been previously reported to interact with other proteins, including Usher type I proteins (reviewed in 17). Harmonin (Usher 1C) is predicted to interact with Usher type I and type II gene products via the PDZ domain and to serve as PDZ domain-based scaffolds to anchor Usher proteins to F-actin (27,28). A link between Usher gene products and actin-based organelles also has been established *in vivo* (reviewed in 17). In this report we show that the F-actin-enriched stereocilia of cochlear hair cells are abnormal in the *Clrn1*<sup>-/-</sup> mice. Regulation and homeostasis of actin filaments is a fundamental process affecting various developmental and functional processes in a multicellular organism. Therefore, one possible molecular mechanism for the observed phenotype in *Clrn1*<sup>-/-</sup> mice might be linked to defective organization/function of actin filaments in the hair cells and neuronal cells. We plan to test this hypothesis in future experiments.

In conclusion, the *Clrn1*<sup>-/-</sup> mouse reported here provides a useful model for inner ear dysfunction in USH3A and to understand the function of CLRN1 in the hair cells and associated neurons. Disabling mutations in *Clrn1* causes clear structural defects in OHCs and affects IHC and OHC function.

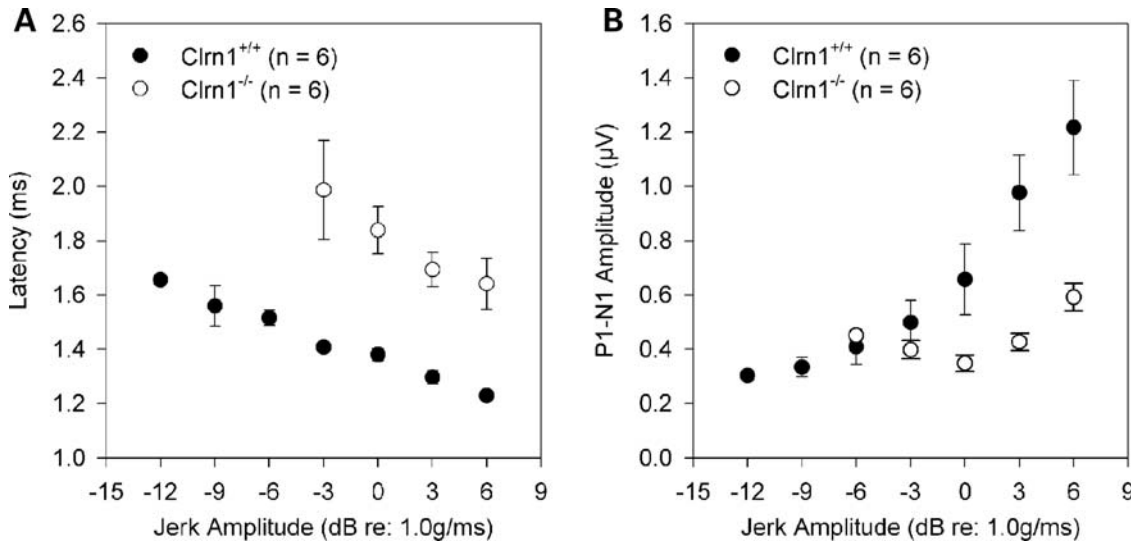


**Figure 6.** VSEP recordings in *Clrn1*<sup>+/+</sup> and *Clrn1*<sup>-/-</sup> mice. Mean P1 latencies (A) and peak-to-peak amplitudes for P1-N1 (B) as a function of increasing levels of jerk. P1-N1 is generated by the peripheral vestibular nerve. *Clrn1*<sup>-/-</sup> animals showed significantly prolonged latencies and significantly reduced amplitudes compared with *Clrn1*<sup>+/+</sup> animals. Error bars represent SEM.

Prolonged peak latencies in vestibular and cochlear evoked potentials strongly suggest that *Clrn1* is necessary for normal sensory transduction, hair cell to afferent communication and/or primary afferent neural activation.

## MATERIALS AND METHODS

### Transgenic targeting of the *Clrn1* gene

A *Clrn1* KO mouse was generated by IngenKO, Pty. Ltd. (Clayton, Victoria, Australia). Briefly, the targeting construct was produced by using the ET cloning system (29) with C57BL/6J genomic DNA. The construct was designed such that loxP sites flanked part of the *Clrn1* upstream promoter, the 5'-UTR, the coding part of the first exon (exon 1), 269 bp of the first intron and a neomycin resistance gene (NeoR). Standard protocol was used to generate cre-mediated targeted deletion of exon 1. The targeting construct was subsequently electroporated into C57BL/6J embryonic stem (ES) cells and recombinant clones were selected using G418. Selected clones were transfected with Cre recombinase and screened by PCR for removal of the *Clrn1* gene fragment noted above. Recombined ES cells were microinjected into BALB/c blastocysts and implanted into pseudo-pregnant mothers. Chimeric progeny were obtained, and highly chimeric animals were subsequently mated with C57BL/6J mice to identify germ-line transmission of the *Clrn1* deletion. Founder animals were identified, and heterozygous progeny were delivered to the University of California, Berkeley (UCB). *Clrn1*<sup>-/-</sup> mice derived from mating *Clrn1*<sup>+/-</sup> mice were sent to Case Western Reserve University (CWRU) for further evaluation. The new allele described in this report was maintained by crossing it to the C57BL/6J (B6) strain, which was used in all parts of this study. The Animal Care and Use Committee at CWRU approved the care and use of the mice included in this investigation.

### Genotyping

A PCR-based protocol was used to identify *Clrn1*<sup>+/+</sup>, *Clrn1*<sup>+/-</sup> and *Clrn1*<sup>-/-</sup> mice. Genomic DNA was isolated from mouse tails by using the Qiagen DNeasy Blood & Tissue Kit. The primers used for genotyping were C1: 5'-TTTACCGAAGCCTTTTCTCG-3'; P3: 5'-GGAGTAAGAAGTAGTCAACGG-3'; and P4: 5'-GCATTTCTCAGCAGATCAC. PCR was carried out at an annealing temperature of 55°C for 35 cycles. PCR products were resolved in 1.5% agarose gels. The genotypes of *Clrn1*<sup>+/+</sup>, *Clrn1*<sup>+/-</sup> and *Clrn1*<sup>-/-</sup> mice were distinguished by PCR (Fig. 3B). In PCR reactions with P3/P4 primers, only a 782 bp band was detected in KO mice, while a 2 kb band was the only band present in *Clrn1*<sup>+/+</sup> mice; the genotype was further confirmed by PCR with C1/P4 primers. Since the C1 primer sequence is located in the first exon, a 1 kb band present in samples from *Clrn1*<sup>+/+</sup> and *Clrn1*<sup>+/-</sup> was not detected in *Clrn1*<sup>-/-</sup> mice.

### Anatomical analyses

For morphological studies of the sequence of postnatal degenerative changes occurring in the inner ears of *Clrn1*<sup>-/-</sup> mutants, mice were examined at each of five time points (2, 5, 10, 20 and 30 days of age). Five *Clrn1*<sup>-/-</sup> mice plus at least two *Clrn1*<sup>+/-</sup> controls per time point were processed for histological analysis. In all cases, inner ear tissues were processed using standard procedure (10).

Methods used for SEM have been described elsewhere (20,21). *Clrn1*<sup>-/-</sup> mice with age-matched control specimens (heterozygous littermates) were studied by SEM at each of four time points (P2, P5, P10 and P15).

### Electroretinograms

ERGs were recorded as described previously (30).

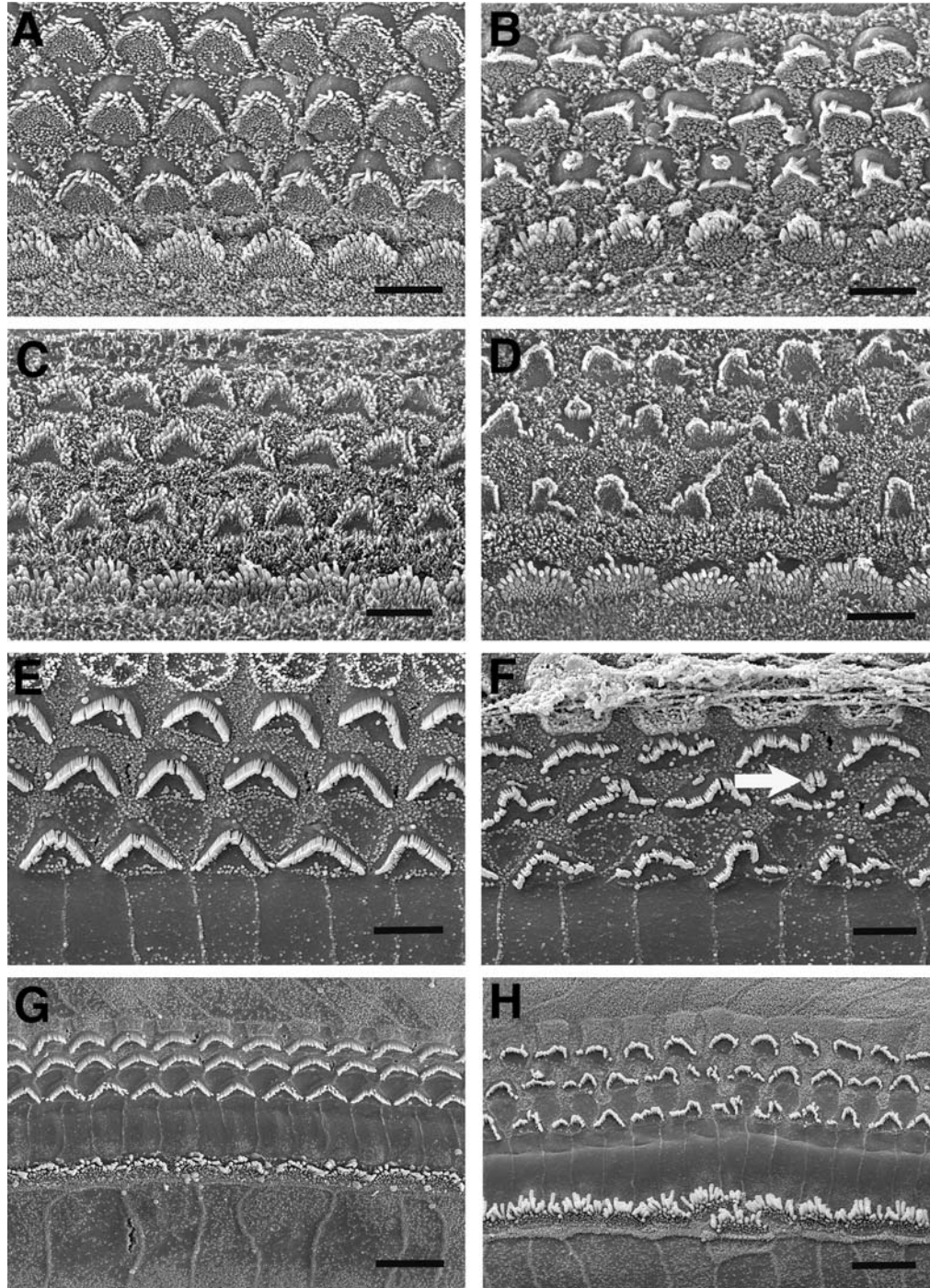


**Figure 7.** Scanning electron micrographs showing surface views of the organ of Corti in *Clrn1*<sup>+/+</sup> and *Clrn1*<sup>-/-</sup> mice aged P2 through P15. Relative to *Clrn1*<sup>+/+</sup> (shown in left column) the OHCs from the *Clrn1*<sup>-/-</sup> animals (right column) show abnormally arranged stereocilia. (A and B) P2; (C and D) P6; (E and F) P10; (G and H) P15. All micrographs taken from basal cochlear turn, except (G and H) which show mid-basal and lower apical turns, respectively. The arrow in (F) indicates a circular cluster of stereocilia (a feature occasionally seen on OHC in the mutants). Scale bars in (A–F) indicate 5  $\mu$ m; scales bars in (G) and (H) indicate 10  $\mu$ m.

### Auditory-evoked brain stem responses

ABR recording was conducted as previously described (31). To test hearing function, *Clrn1*<sup>-/-</sup> mice were presented with broadband clicks or pure tone stimuli at 8, 16 or 32 kHz. *Clrn1*<sup>+/+</sup> [number (*n*) of animals with this genotype

tested = 20], *Clrn1*<sup>+/-</sup> (*n* = 10) and *Clrn1*<sup>-/-</sup> (*n* = 60) mice were analyzed. Click stimuli of 100  $\mu$ s duration were presented for at least 500 sweeps to both the left and right ears (one at a time) through high frequency transducers (a closed system). ABR thresholds were reported as dB peSPL

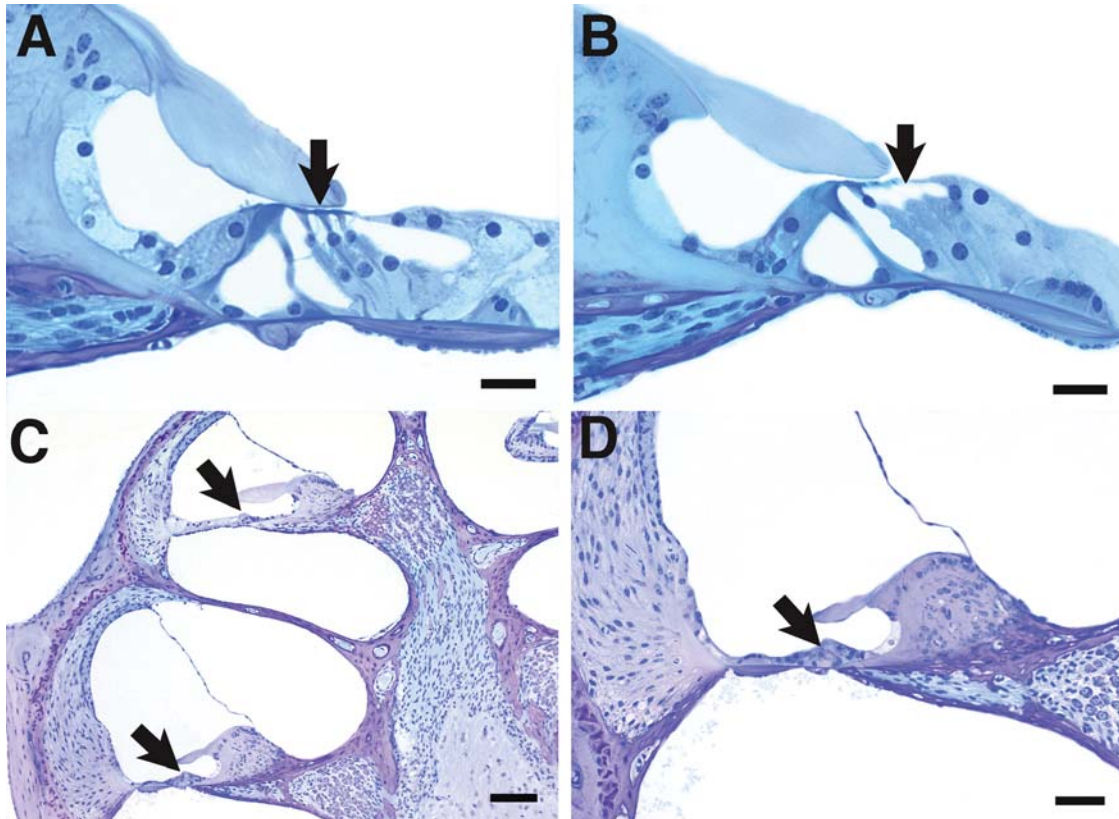


**Figure 8.** Light micrographs showing cochlear cross sections from animals at P21 (A and B) and P30 (C and D). The P21 wild-type specimen (A) shows three rows of OHCs (arrow); however, in the mutant (B), the second and third row OHCs are missing (area indicated by arrow). At P30 all cochlear structures appear normal with the exception of the organ of Corti (arrows in C), which is undergoing degeneration in both the apical and basal turns. (D) Higher power view from the basal turn area at lower left in (A) demonstrating degeneration and collapse of the organ of Corti (arrow). Scales bars in (A and B) indicate 20  $\mu\text{m}$  bars in (C and D) indicate 50  $\mu\text{m}$ .

(identifies how the transient tone burst stimuli were calibrated) were obtained from both ears for each animal by reducing the stimulus intensity from 100 dB peSPL in 10 dB steps; this sequence was repeated in 5 dB steps until the lowest intensity that evoked a reproducible ABR pattern was detected.

#### DPOAE measurements

The basic protocol used for DPOAE recording has been described elsewhere (32,33). The main functional measure used in this study was the 2f<sub>1</sub>-f<sub>2</sub> DPOAE. Briefly, the f<sub>1</sub> and f<sub>2</sub> primary tones were generated by a synthesizer [Tucker-Davis Technologies (TDT, FL)] and attenuated under computer control by using TDT software. The f<sub>1</sub> and f<sub>2</sub> primaries (f<sub>1</sub>/f<sub>2</sub> = 1.2) were then presented over two separate transducers with a 10 dB difference in intensity, f<sub>1</sub> being 10 dB higher than f<sub>2</sub>, and delivered to the outer ear canal through an acoustic probe (Etymotic Research, ER-10B+, Elk Grove Village, IL), where they were allowed to acoustically mix. Ear-canal sound pressure levels were measured by the ER-10B+ emissions microphone assembly embedded in the probe. Corresponding NFs were computed by averaging the levels of the ear-canal sound pressure for five frequency bins above and below the 2f<sub>1</sub>-f<sub>2</sub> DPOAE frequency bin (i.e.  $\pm 54$  Hz). DPOAEs, considered present when they were at

least 3 dB above the NF, are represented as input/output (I/O) functions: the input at the f<sub>1</sub> level (x-axis) is plotted against the output, represented as the mean ( $\pm$  SD) DPOAE levels (y-axis), at these two frequency pairs, i.e. 16-13.3 and 8-6.6 kHz. For I/O testing, data were averaged from 5<sup>+/+</sup> and 5<sup>-/-</sup> mice; results then were compared with the averaged NF from five trials (n = 5).

#### Vestibular evoked potentials

The use of animals for VsEPs was approved at East Carolina University. Mice were anesthetized with a ketamine (90 mg/kg) and xylazine (10 mg/kg) solution and core body temperature was maintained at  $37.0 \pm 0.1^\circ\text{C}$  with a homeothermic heating blanket system (FHC, Inc.). Recording electrodes were placed subcutaneously at the nuchal crest (non-inverting), the pinna (inverting) and the hip (ground). VsEPs were obtained at P14 (WT, n = 4; KO, n = 1), P21 (WT, n = 2; KO, n = 7), P25 (KO, n = 3; WT, n = 3), P30 (KO, n = 3; WT, n = 3) and at 3-6 months of age (KO, n = 3). VsEP recording procedures followed methods described previously (34-36). Here we used a non-invasive spring clip to couple the head to a voltage-controlled mechanical shaker that delivered stimuli to the head. Linear acceleration pulses (2 ms duration, 17 pulses/s) were presented to the cranium

in the naso-occipital axis by using two stimulus polarities, normal (upward) and inverted (initial downward movement). Stimulus amplitude ranged from +6 to -18 dB re: 1.0 g/ms (where 1.0 g = 9.8 m/s<sup>2</sup>) adjusted in 3 dB steps. Ongoing electroencephalographic activity was amplified (200 000×), filtered (300–3000 Hz, -6 dB amplitude points) and digitized (1024 points, 10 μs/point). Primary responses (256) were averaged and replicated for each VsEP waveform. VsEP recordings began at the maximum stimulus intensity (i.e. +6 dB re: 1.0 g/ms) with and without acoustic masking (broadband forward masker 50–50 000 Hz at 97 dB SPL), then the intensity was dropped to -18 dB and subsequently raised in 3 dB steps to complete an intensity profile. The masker was used to verify the absence of auditory components in the VsEP waveform. The first three positive and negative response peaks were scored. Peak latencies (measured in ms), peak-to-peak amplitudes (measured in μV) and thresholds (measured in dB re: 1.0 g/ms) were quantified. Descriptive statistics were generated and the independent samples *t*-test (assuming unequal variances) was used to compare VsEP response parameters between *Cln1*<sup>-/-</sup> and *Cln1*<sup>+/+</sup> mice.

#### Reverse transcriptase-polymerase chain reaction

RT-PCR was used to screen for *Cln1* mRNA in the inner ears of the *Cln1*<sup>-/-</sup> and *Cln1*<sup>+/+</sup> mice. RT-PCR protocol was carried out as described previously (9). RT-PCR was used to amplify various exon combinations of *Cln1* (Fig. 3D). Primers used for this work were C1: 5'-TTTACCGAAGCCTTTTCTCG-3'; C2: 5'-TATGGACTTCCTTG GCCAC-3'; C3: 5'-AGGTACTCTCTGTATGAGGACAA-3'; C4: 5'-TCTTCTCCATGATTCTTGTCGTCT-3'. The following PCR conditions were used: 94°C for 2 min followed by 34 cycles of 30 s each, 55°C for 30 s and 72°C for 1 min. All PCR products were resolved on 3% low range ultra agarose gels (BIO-RAD) and stained with 5% ethidium bromide. Three bands of the following sizes were expected: 834, 780 and 650 bp. Sequences of RT-PCR products were determined with BigDye Terminator Cycle sequencing reagents and protocols (Applied Biosystems, CA). The ABI Prism 377 DNA sequencer (Applied Biosystems) was used to analyze and display the resulting sequence data.

#### In situ hybridization

Animals were housed in the Department of Comparative Medicine at the University of Washington and were euthanized according to approved protocols. Timed pregnant female mice were sacrificed and embryos removed at E16.5 and E18.5. Embryos were fixed in a modified Carnoy's solution (60% ethanol:4% formaldehyde:10% acetic acid) overnight at 4°C. Specimens were washed and dehydrated in 100% ethanol overnight at 4°C and then embedded in paraffin; 6 mm sections were subsequently cut and collected. For the postnatal mice, we assigned the day of birth as postnatal day 0 (P0) and sacrificed pups at P0, P3 and P5, according to approved protocols. We then dissected the cochleas from these animals, fixed them and processed them for paraffin sectioning as described above. At least three animals were

examined for each time point. Mouse *Cln1* cDNA (clone ID: 40130533) was obtained from Open Biosystems Inc. A full-length clone containing exons 1 and 4 with 3' and 5'-UTRs was used as the template to generate Digoxigenin (DIG)-labeled probes, which were prepared according to the manufacturer's manual for DIG-11-UTP (Roche, Indianapolis, IN); hybridizations were then carried out according to Hayashi *et al.* (37). *In situ* products were visualized by using anti-DIG alkaline phosphatase-conjugated secondary antibody (Roche) and the NBT/BCIP liquid substrate system (Sigma, St Louis, MO). After *in situ* hybridization, slides were fixed with 4% paraformaldehyde for 1 h and washed in PBS. Slides then were incubated with 10% fetal bovine serum and 2% non-fat dry milk in PBS/0.1% Triton X-100 (PBST) for 30 min. After overnight incubation with the primary antibody [rabbit anti-Myosin6 (Myo6, Proteus Biosystems)] at 1:2000 dilution, or rabbit anti-β-tubulin III (TuJ1, Covance, Austin, TX) at 1:1000 dilution, slides were washed and incubated in fluorescent-conjugated secondary antibody, rinsed with PBST and cover-slipped in Fluoromount G (Southern Biotechnology, Birmingham, AL). Images were captured by a Zeiss Axioplan microscope with a SPOT CCD camera and processed by using Adobe Photoshop.

#### AUTHORS' CONTRIBUTIONS

R.G., T.H., C.R., T.A.R., O.B.-McD., S.M.J., C.G.W. and K.N.A. contributed in experimental design, experiments and data analysis; S.M. performed DPOAE data analysis; Y.I. and K.P. research design; S.F.G. and J.G.F. designed and generated the clarin-1 knockout mouse; R.G. and K.N.A. wrote the paper.

#### ACKNOWLEDGEMENTS

The authors thank the technical support provided by Daniel Chen in K.N.A.'s laboratory. We thank Dr Kermany of the Center for Hearing & Deafness, U. Buffalo for technical support with DPOAE recordings and analysis. We thank Brian McDermott for critically reviewing the manuscript. We would like thank Guilian Tian (YI's lab) and Tadao Maeda in the Ophthalmology department, CWRU, for technical support with ERG analysis.

*Conflict of Interest statement.* None declared.

#### FUNDING

This work was supported by the Hope for Vision Foundation to K.N.A., Y.I., J.G.F., O.B.-McD. and T.R. and by National Institutes of Health R01 DC006443 to S.M.J.

#### REFERENCES

- Petit, C. (2001) Usher syndrome: from genetics to pathogenesis. *Annu. Rev. Genomics Hum. Genet.*, **2**, 271–297.
- Kremer, H., van Wijk, E., Marker, T., Wolfrum, U. and Roepman, R. (2006) Usher syndrome: molecular links of pathogenesis, proteins and pathways. *Hum. Mol. Genet.*, **15** (Spec no. 2), R262–R270.

3. Reiners, J., Nagel-Wolfrum, K., Jurgens, K., Marker, T. and Wolfrum, U. (2006) Molecular basis of human Usher syndrome: deciphering the meshes of the Usher protein network provides insights into the pathomechanisms of the Usher disease. *Exp. Eye Res.*, **83**, 97–119.
4. Adato, A., Vreugde, S., Joensuu, T., Avidan, N., Hamalainen, R., Belenkiy, O., Olender, T., Bonne-Tamir, B., Ben-Asher, E., Espinos, C. *et al.* (2002) USH3A transcripts encode clarin-1, a four-transmembrane-domain protein with a possible role in sensory synapses. *Eur. J. Hum. Genet.*, **10**, 339–350.
5. Hemler, M.E. (2003) Tetraspanin proteins mediate cellular penetration, invasion, and fusion events and define a novel type of membrane microdomain. *Annu. Rev. Cell. Dev. Biol.*, **19**, 397–422.
6. Hemler, M.E. (2005) Tetraspanin functions and associated microdomains. *Nat. Rev. Mol. Cell. Biol.*, **6**, 801–811.
7. Hubner, K., Windoffer, R., Hutter, H. and Leube, R.E. (2002) Tetraspanin vesicle membrane proteins: synthesis, subcellular localization, and functional properties. *Int. Rev. Cytol.*, **214**, 103–159.
8. Chen, L., Chetkovich, D.M., Petralia, R.S., Sweeney, N.T., Kawasaki, Y., Wenthold, R.J., Bredt, D.S. and Nicoll, R.A. (2000) Stargazin regulates synaptic targeting of AMPA receptors by two distinct mechanisms. *Nature*, **408**, 936–943.
9. Alagramam, K.N., Murcia, C.L., Kwon, H.Y., Pawlowski, K.S., Wright, C.G. and Woychik, R.P. (2001) The mouse Ames waltzer hearing-loss mutant is caused by mutation of Pcdh15, a novel protocadherin gene. *Nat. Genet.*, **27**, 99–102.
10. Alagramam, K.N., Zahorsky-Reeves, J., Wright, C.G., Pawlowski, K.S., Erway, L.C., Stubbs, L. and Woychik, R.P. (2000) Neuroepithelial defects of the inner ear in a new allele of the mouse mutation Ames waltzer. *Hear. Res.*, **148**, 181–191.
11. Zhou, R., Assouline, J.G., Abbas, P.J., Messing, A. and Gantz, B.J. (1995) Anatomical and physiological measures of auditory system in mice with peripheral myelin deficiency. *Hear. Res.*, **88**, 87–97.
12. Jones, S.M., Johnson, K.R., Yu, H., Erway, L.C., Alagramam, K.N., Pollak, N. and Jones, T.A. (2005) A quantitative survey of gravity receptor function in mutant mouse strains. *J. Assoc. Res. Otolaryngol.*, **6**, 297–310.
13. Pennings, R.J., Fields, R.R., Huygen, P.L., Deutman, A.F., Kimberling, W.J. and Cremers, C.W. (2003) Usher syndrome type III can mimic other types of Usher syndrome. *Ann. Otol. Rhinol. Laryngol.*, **112**, 525–530.
14. Ness, S.L., Ben-Yosef, T., Bar-Lev, A., Madeo, A.C., Brewer, C.C., Avraham, K.B., Kornreich, R., Desnick, R.J., Willner, J.P., Friedman, T.B. *et al.* (2003) Genetic homogeneity and phenotypic variability among Ashkenazi Jews with Usher syndrome type III. *J. Med. Genet.*, **40**, 767–772.
15. Nayak, G.D., Ratnayaka, H.S., Goodyear, R.J. and Richardson, G.P. (2007) Development of the hair bundle and mechanotransduction. *Int. J. Dev. Biol.*, **51**, 597–608.
16. Geleoc, G.S., Risner, J.R. and Holt, J.R. (2004) Developmental acquisition of voltage-dependent conductances and sensory signaling in hair cells of the embryonic mouse inner ear. *J. Neurosci.*, **24**, 11148–11159.
17. Brown, S.D., Hardisty-Hughes, R.E. and Mburu, P. (2008) Quiet as a mouse: dissecting the molecular and genetic basis of hearing. *Nat. Rev. Genet.*, **9**, 277–290.
18. El-Amraoui, A. and Petit, C. (2005) Usher I syndrome: unravelling the mechanisms that underlie the cohesion of the growing hair bundle in inner ear sensory cells. *J. Cell Sci.*, **118**, 4593–4603.
19. Lefevre, G., Michel, V., Weil, D., Lepelletier, L., Bizard, E., Wolfrum, U., Hardelin, J.P. and Petit, C. (2008) A core cochlear phenotype in USH1 mouse mutants implicates fibrous links of the hair bundle in its cohesion, orientation and differential growth. *Development*, **135**, 1427–1437.
20. Kikkawa, Y.S., Pawlowski, K.S., Wright, C.G. and Alagramam, K.N. (2008) Development of outer hair cells in Ames waltzer mice: mutation in protocadherin 15 affects development of cuticular plate and associated structures. *Anat. Rec. (Hoboken)*, **291**, 224–232.
21. Pawlowski, K.S., Kikkawa, Y.S., Wright, C.G. and Alagramam, K.N. (2006) Progression of inner ear pathology in Ames waltzer mice and the role of protocadherin 15 in hair cell development. *J. Assoc. Res. Otolaryngol.*, **7**, 83–94.
22. Liu, X., Bulgakov, O.V., Darrow, K.N., Pawlyk, B., Adamian, M., Liberman, M.C. and Li, T. (2007) Usherin is required for maintenance of retinal photoreceptors and normal development of cochlear hair cells. *Proc. Natl. Acad. Sci. USA*, **104**, 4413–4418.
23. Mburu, P., Mustapha, M., Varela, A., Weil, D., El-Amraoui, A., Holme, R.H., Rump, A., Hardisty, R.E., Blanchard, S., Coimbra, R.S. *et al.* (2003) Defects in whirlin, a PDZ domain molecule involved in stereocilia elongation, cause deafness in the whirler mouse and families with DFNB31. *Nat. Genet.*, **34**, 421–428.
24. McGee, J., Goodyear, R.J., McMillan, D.R., Stauffer, E.A., Holt, J.R., Locke, K.G., Birch, D.G., Legan, P.K., White, P.C., Walsh, E.J. *et al.* (2006) The very large G-protein-coupled receptor VLRG1: a component of the ankle link complex required for the normal development of auditory hair bundles. *J. Neurosci.*, **26**, 6543–6553.
25. Maerker, T., van Wijk, E., Overlack, N., Kersten, F.F., McGee, J., Goldmann, T., Sehn, E., Roepman, R., Walsh, E.J., Kremer, H. *et al.* (2008) A novel Usher protein network at the periciliary reloading point between molecular transport machineries in vertebrate photoreceptor cells. *Hum. Mol. Genet.*, **17**, 71–86.
26. Adato, A., Kalinski, H., Weil, D., Chaib, H., Korostishevsky, M. and Bonne-Tamir, B. (1999) Possible interaction between USH1B and USH3 gene products as implied by apparent digenic deafness inheritance. *Am. J. Hum. Genet.*, **65**, 261–265.
27. Boeda, B., El-Amraoui, A., Bahloul, A., Goodyear, R., Daviet, L., Blanchard, S., Perfettini, I., Fath, K.R., Shorte, S., Reiners, J. *et al.* (2002) Myosin VIIa, harmonin and cadherin 23, three Usher I gene products that cooperate to shape the sensory hair cell bundle. *Embo J.*, **21**, 6689–6699.
28. Adato, A., Michel, V., Kikkawa, Y., Reiners, J., Alagramam, K.N., Weil, D., Yonekawa, H., Wolfrum, U., El-Amraoui, A. and Petit, C. (2005) Interactions in the network of Usher syndrome type I proteins. *Hum. Mol. Genet.*, **14**, 347–356.
29. Angrand, P.O., Daigle, N., van der Hoeven, F., Scholer, H.R. and Stewart, A.F. (1999) Simplified generation of targeting constructs using ET recombination. *Nucleic Acids Res.*, **27**, e16.
30. Maeda, A., Maeda, T., Imanishi, Y., Kuksa, V., Alekseev, A., Bronson, J.D., Zhang, H., Zhu, L., Sun, W., Saperstein, D.A. *et al.* (2005) Role of photoreceptor-specific retinol dehydrogenase in the retinoid cycle *in vivo*. *J. Biol. Chem.*, **280**, 18822–18832.
31. Megerian, C.A., Semaan, M.T., Aftab, S., Kisley, L.B., Zheng, Q.Y., Pawlowski, K.S., Wright, C.G. and Alagramam, K.N. (2008) A mouse model with postnatal endolymphatic hydrops and hearing loss. *Hear. Res.*, **237**, 90–105.
32. Jimenez, A.M., Stagner, B.B., Martin, G.K. and Lonsbury-Martin, B.L. (1999) Age-related loss of distortion product otoacoustic emissions in four mouse strains. *Hear. Res.*, **138**, 91–105.
33. Martin, G.K., Vazquez, A.E., Jimenez, A.M., Stagner, B.B., Howard, M.A. and Lonsbury-Martin, B.L. (2007) Comparison of distortion product otoacoustic emissions in 28 inbred strains of mice. *Hear. Res.*, **234**, 59–72.
34. Jones, S.M., Erway, L.C., Johnson, K.R., Yu, H. and Jones, T.A. (2004) Gravity receptor function in mice with graded otoconial deficiencies. *Hear. Res.*, **191**, 34–40.
35. Jones, T.A. and Jones, S.M. (1999) Short latency compound action potentials from mammalian gravity receptor organs. *Hear. Res.*, **136**, 75–85.
36. Jones, S.M., Subramanian, G., Avniel, W., Guo, Y., Burkard, R.F. and Jones, T.A. (2002) Stimulus and recording variables and their effects on mammalian vestibular evoked potentials. *J. Neurosci. Methods*, **118**, 23–31.
37. Hayashi, T., Cunningham, D. and Bermingham-McDonogh, O. (2007) Loss of Fgfr3 leads to excess hair cell development in the mouse organ of Corti. *Dev. Dyn.*, **236**, 525–533.